Remote Sensing of Environment 221 (2019) 1–13

Contents lists available at ScienceDirect

Remote Sensing of Environment

journal homepage: www.elsevier.com/locate/rse

Towards high throughput assessment of canopy dynamics: The estimation of leaf area structure in Amazonian forests with multitemporal multi-sensor airborne lidar

Gang Shao[a,*], Scott C. Stark[a], Danilo R.A. de Almeida[b], Marielle N. Smith[a]

[a] Department of Forestry, Michigan State University, 480 Wilson Rd, East Lansing, MI 48824, United States of America
[b] Department of Forest Sciences, University of São Paulo, "Luiz de Queiroz" College of Agriculture (USP/ESALQ), Av. Pádua Dias, 11, 13418-900 Piracicaba, SP, Brazil

ARTICLE INFO

Keywords:
Lidar
Leaf area estimation
LAI
Leaf area profiles
Forest degradation
Tropical forest monitoring
Forest dynamics

ABSTRACTS

Leaf area dynamics offer information about changes in forest biomass and canopy function critical to understanding the role of forests in the climate system and carbon cycle. Airborne small footprint lidar is a potential major source for the detection of variation in leaf area density (LAD), LAD vertical profiles, and total leaf area (leaf area index, LAI), from sites to regional scales. However, the sensitivities of lidar-based LAD and LAI estimation are not yet well known, particularly in dense forests, over landscape heterogeneity, sensor system, and survey differences, and through time. To address these questions, we compared 16 pairs of multitemporal airborne lidar surveys with four different laser sensors across six Amazon forest sites with resurvey intervals ranging from one to nine years. We tested whether the different laser sensors, and the pulse return density of laser sampling (variable between and within each survey) introduce systematic biases. Laser sensors created consistent biases that accounted for up to 18.20% of LAD differences between surveys, but biases could be corrected with a simple regression approach. Lidar pulse return density had little appreciable bias impact when above 20 returns per m^2. After correction, repeated mean and site maximum LAI estimates became significantly correlated (R^2 ~0.8), while LAD profiles revealed site differences. Heterogeneity and change in LAD structure were detectable at the ecologically relevant 1/4 ha forest neighborhood grid scale, as evidenced by the high correlation of profile variation between surveys, with the strength of correlation (R^2 value) significantly decreasing with increasing survey interval (0.74 to 0.16 from one to nine years), consistent with accumulating effects of forest dynamics. Sensor-induced biases trended towards correlation with lidar footprint (beam width). The LAD estimation and bias correction approach developed in this study provides the standardization critical for heterogeneous lidar networks that offer high throughput functional ecological monitoring of climatically important forests like the Amazon.

1. Introduction

Forest canopies play critical roles in global carbon and water cycles and determine fluxes of heat and energy to the atmosphere that drive atmospheric circulation and influence the climate (Bonan, 2008). However, forests are changing on a global scale due to deforestation, land use change, changing climate, and invasive pests and pathogens, which are substantially altering forest ecosystem services including biomass production, carbon storage, and regional and global climate regulation (Foley et al., 2007; Hansen et al., 2013; Allen et al., 2015; Stark et al., 2016). A key challenge is to develop rapid and large-scale remote monitoring approaches to identify and quantify forests that are sensitive to these different types of change (McDowell et al., 2015; Chambers et al., 2007). The Amazon basin, as the largest tropical forest region, plays a correspondingly important role in regulating Earth's climate system and carbon cycle (Malhi et al., 2008). Increasing drought frequency and intensity may be impacting Amazon forest structure and function (Phillips et al., 2009; Davidson et al., 2012); however, the nature and extent of these impacts remain controversial (e.g., Saleska et al., 2007; Hilker et al., 2014), highlighting the need for accurate monitoring of forest change sensitive to ecological processes and functions (Chambers et al., 2007).

The structure of canopy leaf area can serve as a basis to monitor forest ecological change (Knapp et al., 2018; Asner et al., 2007; Parker et al., 2004b). The quantity and spatial structure of canopy leaf area influences radiation interception and reflectance, and in turn,

* Corresponding author.
E-mail address: shaogang@msu.edu (G. Shao).

https://doi.org/10.1016/j.rse.2018.10.035
Received 21 July 2018; Received in revised form 20 October 2018; Accepted 27 October 2018
Available online 07 November 2018
0034-4257/

production, evapotranspiration, and heat fluxes (Bonan, 2015). Leaf area index (LAI, $m^2 m^{-2}$), defined as the one-sided leaf area per unit ground surface area, is a common measure for leaf quantity and an essential parameter for ecological models, which propagate area-specific measures of leaf function over total leaf area (LAI), and environmental variables, to predict canopy function (Fisher et al., 2007; Garcia et al., 2016; Guo et al., 2015). The vertical and horizontal volumetric distribution of leaf area, leaf area density (LAD, $m^2 m^{-3}$), provides critical information to understand canopy light environments and functions (Parker et al., 2004a; Antonarakis et al., 2014). Canopy profiles of LAD can also reveal the dynamics of woody biomass (Stark et al., 2012), and demographic states and fluxes (Stark et al., 2015) when forest 'neighborhood' scale (i.e., ~1 ha plot scale) heterogeneity is measured. Therefore, the accurate quantification of LAI and LAD is essential to improve monitoring of changing canopy structure and its consequences for ecosystem-atmosphere functions.

LAI and LAD are challenging to measure in forests, particularly at ecologically relevant neighborhood scales, whether employing direct or remote approaches (Olivas et al., 2013). For data sources ranging from field-collected hemispherical photographs to satellite-based spectroradiometers (e.g., MODIS), leaf area is typically estimated by variables that integrate information from the full vertical canopy column—canopy absorption, reflectance, transmittance, or cover—limiting estimation to total leaf area, i.e., LAI, and introducing error associated with high LAI value ($> 5 m^2 m^{-2}$) sensor saturation (Weiss et al., 2004; Zheng and Moskal, 2009; Olivas et al., 2013; Tang et al., 2016). Measuring the spatial structure of LAD, including fully vertically resolved leaf area profiles, has represented the greatest challenge and is possible only through painstaking direct harvesting (Clark et al., 2008), or from canopy penetrating range measurements, which have become more widely available with the advent of laser ranging and lidar (Lefsky et al., 2002; Parker et al., 2004a).

Lidar offers detailed 3-D canopy structural information including LAD vertical profiles and LAI estimates (Hosoi et al., 2010; Stark et al., 2012). LAI and LAD are estimated from laser pulse penetration or interception rates; in this case, the laser ranging light in any volumetric units of canopy space is reflected towards and received by the sensor according to interactions with leaves and other surface area (Parker et al., 2004a; Stark et al., 2012; Detto et al., 2015). Thus, knowledge of the incidence of laser light or laser pulse number and the proportion of light or pulses reflected back provides raw information about surface area density—the largest fraction of which is attributed to leaf area (Lefsky et al., 2002)—within each volumetric unit.

Lidar based approaches have demonstrated great potentials for multi-scale LAI and LAD estimation (Tang et al., 2012; Vincent et al., 2017). In addition, the increasing prevalence of multitemporal (repeated) lidar surveys offers unprecedented opportunities to observe leaf area and forest structural changes over landscapes. However, the accuracy, consistency, and sensitivities of leaf area estimation to lidar survey parameters, such as pulse return densities, remain little explored (Morsdorf et al., 2008; Liu et al., 2018). Due to the diversity of lidar sensors, varied campaign designs, and broad geographical scopes, databases including repeated surveying through time are expected to often include significant variation in terms of lidar sampling. Lidar surveys with different sensor systems, pulse return densities, penetration rates, and laser footprints (and divergences) could introduce biases in leaf area estimation (Véga et al., 2016), but these biases remain poorly understood. To improve understanding of forest structural change, including at finer forest neighborhood scales, validation and standardization of LAI and LAD derived from multitemporal, multi-site, multi-sensor lidar datasets is required.

Here we investigated the capacity of multitemporal airborne lidar, spanning sensor systems, and survey specifications, to consistently and accurately estimate leaf area and its dynamics. We compared estimates from 16 repeated surveys with four commonly used airborne laser sensors in six Brazilian Amazon forest sites, spanning nine survey years. We asked:

- *Overarching question*: Can variation in canopy LAI and LAD structure (particularly vertical profiles) be estimated from a varied multitemporal Amazon forest lidar database with sufficient accuracy to monitor forest change through time and over geographical gradients?
- *Bias correction*: Are there systematic biases in LAI and LAD estimation that can be corrected? And are biases associated with sensor systems or with survey parameters, specifically laser pulse sampling intensity (pulse return density)?
- *Monitoring at the neighborhood scale*: Can multitemporal lidar reveal structural changes in terms of LAD profiles at fine forest neighborhood scales (1/4 ha)? And how does change in neighborhood structure respond to the interval between lidar surveys?

2. Study area and data

2.1. Study area

Our study area included six forest sites in the Brazilian Amazon spanning four states (Fig. 1). All sites are tropical moist forests and include: CAU (Fazenda Cauaxí), FST (Saracá-Taquera National Forest), the TNF (Tapajós National Forest) in Pará, DUC (Adolpho Ducke Forest Reserve) in Amazonas, JAM (Jamari National Forest) located in Rondônia, and the drier FN (Feliz Natal) in Mato Grosso. These sites encompass a variety of forest types, climates, and disturbance histories (Table S1; see Longo et al., 2016 for a detailed description of the disturbance history of each forest site).

2.2. Lidar data

Airborne lidar surveys were conducted as part of the Sustainable Landscapes Brazil project implemented by USFS (the U.S. Forest Service) and EMBRAPA (Brazilian Corporation of Agricultural Research) and supported by USAID (the U.S. Agency for International Development) and the U.S. Department of State (Longo et al., 2016).

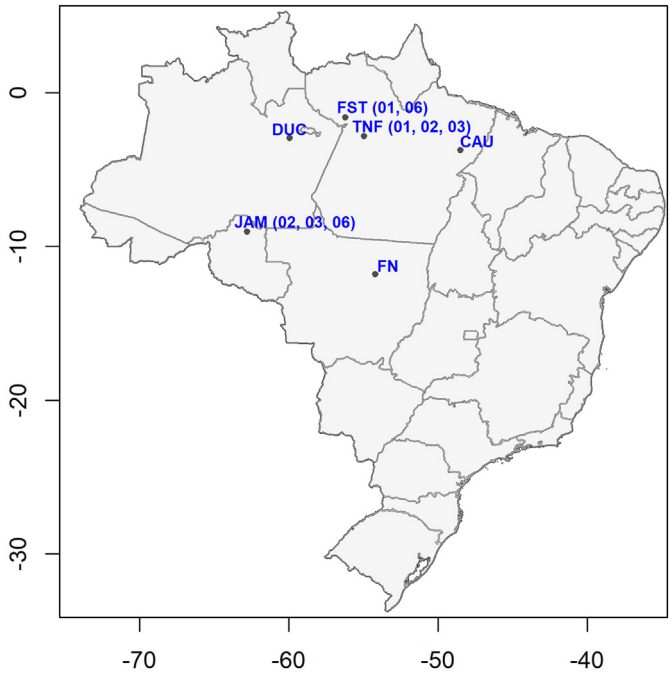

Fig. 1. Locations of the study areas on a map of Brazil, which include 6 forest sites within Brazilian Amazon. The numbers in brackets following the site names are subsite indices.

Table 1
Sensors and surveys.
* The numbers that follow site names are subsite indices.

Sensor	ALS50-II	ALTM 3100	ALTM Orion	Harrier 68i
Survey year	2008	2011, 2012, 2015, 2016, 2017	2013, 2014, 2015	2014
Sites surveyed*	DUC, TNF01	CAU, DUC, FN, JAM02, JAM06, TNF01, TNF02, TNF03	CAU, FN, FST01, FST06, JAM02, JAM03, TNF02, TNF03	FST01, FST06, JAM02, JAM03, JAM06
Beam divergence (mrad)	0.15	0.30	0.25	0.50
Average flying altitude (m)	816	850	850	500
Average footprint (m)	0.122	0.255	0.213	0.250
Maximum scan angle	10°	11°	11°	30°
Point density (pts m^{-2})	51.7–55.5	22.7–66.4	30.0–61.4	42.8–56.1
Average first return ratio (%)	77.8	56.0	54.1	61.9
Flightline overlap (%)	27	65	65	65

The data were collected between 2008 and 2017 with four laser sensors (Table 1): ALS50-II (Leica Geosystems) in 2008, ALTM 3100 (Optech Inc.) in 2012, 2016 and 2017, ALTM Orion (Optech Inc.) in 2013 and 2015, and Harrier 68i (Trimble Navigation) in 2014.

Among these four sensors, ALS50-II has the strongest beam energy and smallest beam divergence (mrad of 0.15) flying at an altitude of about 800 m, a scan angle of 10°, and flightline overlap of 27%, to achieve 51.7 to 55.5 pts m^{-2}. ALTM 3100 and ALTM Orion had slightly different beam divergence values (mrad of 0.30 and 0.25, respectively), but similar collection parameters, with flying altitudes of 700–853 m, maximum scan angles ranging from 10° to 15°, and about 65% flightline overlap. Broadly, average pulse return densities ranged from 22.7 to 66.4 pts m^{-2}. The Harrier 68i had the weakest beam energy (mrad of 0.5). As a result, these surveys were flown at the lowest altitude (500 m) with the largest scan angle (30°) and high flightline overlap (65%), to obtain high return density data (42.8–56.1 pts m^{-2}).

Some of the six forest sites had multiple subsites (Fig. 1) and some had more than two surveys conducted with different laser systems (Table 1), resulting in a total of 16 pairs of multitemporal measurements. Each pair consists of two lidar surveys made at the same site, with the same geographical coverage, in different years, and with different sensors. Our dataset contains all pairwise combinations of ALTM 3100, ALTM Orion and Harrier 68i. However, the ALS50-II was only used in 2008 and followed by ALTM 3100 in 2012 and 2017 at the DUC and the TNF (subsite 1, TNF01); thus, there were no pairs comprising ALS50-II and ALTM Orion or Harrier 68i data (all pair groups are shown in Table S2).

The Sustainable Landscapes survey planners held survey parameters associated with each lidar sensor constant to enhance comparability. As such aircraft relative altitude and other parameters varied over lidar sensors, but varied little among the specific site surveys conducted by each sensor. Thus, sensor induced biases, as we consider them, could be influenced by survey parameters and sensor characteristics (Section 3.7).

3. Methodology

Two primary methodological steps were needed to achieve our objectives: 1.) Quantify and correct leaf area estimation biases caused by lidar sensor and pulse return density variation; and 2.) Evaluate the detection of structural changes with corrected leaf area estimates using multitemporal lidar surveys. To quantify and correct leaf area estimation biases, we first estimated LAD at a fine scale (2 × 2 × 1 m voxels) (see Fig. 2 method summary). Then, we aggregated LAD estimates to the forest neighborhood scale, while maintaining vertical resolution (1/4 ha grid cells, or 50 × 50 × 1 m voxels), and calculated the total LAI value of each 1/4 ha grid cell. With these multitemporal leaf area estimates (LAIs and LAD profiles) at the forest neighborhood scale, we investigated the potential of sensor-induced and pulse return density-related biases, and produced a bias correction routine with a conceptual model explained in Section 3.3. To assess structural changes with corrected leaf area estimates, we explored possible connections between surface height changes and leaf area changes, and we applied regression analysis to multitemporal leaf area variation (deviations from regular vertical patterns). Thus, we tested the detectability and consistency of LAD variation in neighborhoods through time. We also asked if survey (sensor) parameters correlated with biases.

3.1. Lidar data processing

First, outliers of lidar point clouds were identified and removed by restricting lidar pulse returns within three standard deviations of mean elevations (Fig. 2). Then, lidar pulse return counts were tallied in voxels (voxelization) with a 2 × 2 m horizontal and 1 m vertical grid scale (i.e., 3-D analog to pulse tally rasterization). Digital terrain models (DTMs) were determined for each survey using minimum quantile spline regression and interpolation (See 'Ground surface estimation' in Supplementary material). Based on the DTMs, 3-D voxel data were 'leveled' to aboveground height so that the lowest voxel represented the ground for all datasets—similar conceptually to the 'leveling' step that produces canopy height models (CHMs) by subtracting DTMs from digital surface models (DSMs). LAD estimates at the fine scale (2 × 2 × 1 m) were then used to estimate average vegetation density profiles and LAD values at the 1/4 ha forest neighborhood scale (50 × 50 × 1 m). Areas not penetrated by lidar pulses did not contribute to horizontal averages. The vertical dimension was set at 1 m to enhance representation of vertical variation, relevant for analysis of forest dynamics (Stark et al., 2012, 2015). The 50 × 50 m horizontal grid cell is also the scale of field inventory plots in the study region. All analyses were conducted in R (R Development Core Team, v3.3.2, 2013).

3.2. Leaf area density (LAD) estimation

Our approach to estimate LAD follows foundational work applying lidar in ecosystem studies (Harding et al., 1994; Lefsky et al., 2002; Parker et al., 2004a), and earlier active canopy probe leaf area estimation methods (MacArthur and Horn, 1969; Aber, 1979). Within each 2 × 2 × 1 m voxel, LAD was estimated from vertical transmission rates of lidar pulses. Leaf area per unit volume (LAD_i) estimates were calculated as:

$$LAD_i = ln\left(\frac{P_{in}}{P_{out}}\right)\frac{1}{k\Delta z}$$

where P_{in} is the number of laser pulses entering voxel i (omitting horizontal indexing for clarity) from the direction of the lidar device, P_{out} is the number of pulses exiting the voxel on the other side, Δz is the vertical dimension (1 m in this study), and k is an adjustment factor relating leaf area to the pulse interception, reflection, and detection probability. This equation can also be interpreted as the natural log of the inverse of pulse transmission rate scaled to best estimate leaf area in

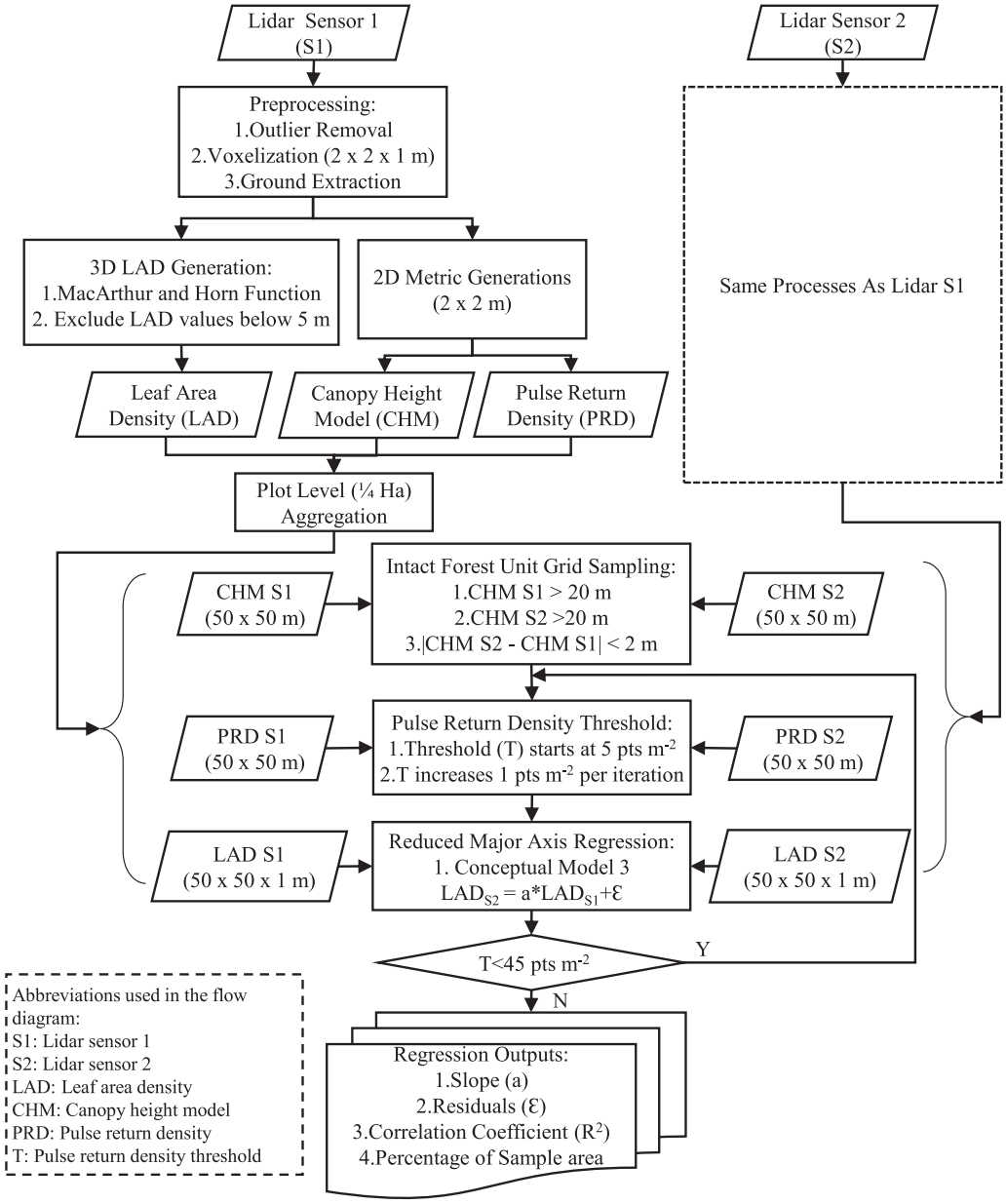

Fig. 2. Flow diagram for the identification and correction of sensor-induced bias of LAD estimation.

the Amazonian forest.

The leaf area scaling constant *k*, was set through reference to an independently estimated LAI value. We compared published estimates of the LAI of the TNF (average of $5.72\,m^2\,m^{-2}$) based on non-lidar methods (Stark et al., 2012; from references summarized therein) with our estimates of LAI derived from the first (2008) Leica AL50-II lidar survey, and found *k* to be 0.803. To improve accuracy, we excluded LAD estimates below 5 m, which were more uncertain because of limited pulse penetration low in the canopy (Stark et al., 2012); based on prior work and preliminary results we assumed that this would reduce total reference LAI by $0.25\,m^2\,m^{-2}$.

3.3. Conceptual model for leaf area bias correction

We investigated multiple potential sources of bias influencing our ability to estimate leaf area—both LAD and LAI—with lidar sensors. We considered the potential for biases to be caused by, (*i*) the properties of the lidar sensor (and associated survey parameters) influencing the sensitivity of LAD estimation (termed as sensor-induced bias in the following sections). We then consider (*ii*) whether bias is associated with the density of lidar pulses (measured here as the pulse return density), which unlike other lidar parameters can be highly spatially variable within surveys. We built a mathematical-conceptual model to disentangle these sources of bias, and then applied it to comparisons of leaf area estimates of lidar survey pairs at 1/4 ha neighborhood scales.

Start by assuming that given unbiased LAD estimation in repeat surveys, estimates in a second survey (LAD_{y2}) would equal those of the first survey (LAD_{y1}), plus any changes in the LAD at the same vertical position in the canopy (C1):

Model 1: $LAD_{y2} = LAD_{y1} + C1$

If the different lidar sensors have different sensitivities, this would introduce a bias (e1) in Model 1 for each device pair. Furthermore, if pulse return density (PRD) variation causes bias, then both devices' PRDs will influence combined bias for this factor, which we model as the additive term e2:

Model 2: $LAD_{y2} = (1+e1)*LAD_{y1} + C1 + e2\,(PRD_{y1}, PRD_{y2})$

LAD comparisons from survey pairs in intact undisturbed forest should not display consistent LAD changes (C1 = 0), and thus should be linearly related and pass through the origin. Model 3 summarizes, where sensor-induced bias factor, a = 1 + e1, and pulse return density related bias, Ɛ ~e2(PRD_{y1}, PRD_{y2}):

Model 3: $LAD_{y2} = a*LAD_{y1} + Ɛ$

Applying linear regression analysis to this model within unchanging intact forest regions (see Supplementary material 'Grid Cell Filtering Approach'). The stability of the regression slope would reflect the consistency of sensor-sensitivity induced biases, while model residuals would be related to pulse return densities in both surveys.

3.4. Assessing pulse return density related and sensor-induced biases

We evaluated pulse return density as a source of LAD profile bias in survey pairs (Fig. 2). The range of pulse return densities in our dataset —22 to 66 pts m^{-2}—is considered high and adequate for accurate lidar metric estimation, particularly for canopy surface attributes (Jakubowski et al., 2013; Silva et al., 2017; Wulder et al., 2012; Zhao et al., 2018). Instead of comparing pulse return density variation between survey pairs, our study mainly focused on the variation in pulse return density within each survey among grid cells, which ranged from 3 to over 100 pts m^{-2} (Supplementary material, 'Direct pulse return density-related bias assessment'). Analyses were conducted on forest neighborhoods filtered for mature forests (mean canopy height > 20 m) that had not undergone disturbance impacting the canopy surface height (i.e., had < 2 m of canopy surface height change; Supplementary material, 'Grid cell filtering approach').

We tested for pulse return density-related bias by exploring variation of regression parameters over variation in pulse return density requirements (see Supplementary material for a second approach, 'Direct pulse return density-related bias assessment.'). We applied a sliding filter of minimum acceptable pulse density sampling 'threshold values'—a higher pulse return density threshold value may indicate higher data quality for leaf area estimation but it is more restrictive, reducing the number of neighborhoods available for analysis. As we varied the pulse return density threshold, we tracked sensor induced biases (slopes), residuals, and R^2 values of fits of Model 3. We hypothesized that if pulse return density creates bias we would observe strong shifts in residuals. Furthermore, if sensor induced bias is impacted by pulse return density, regression slopes should shift as well. The absence of a shift, however, would support Model 3's partitioning of sensor induced and pulse return density related bias.

To estimate sensor-induced bias we also have to identify an optimal pulse return density threshold; this would be the smallest value that corresponds with a stable regression slope (sensor-induced bias), stable R^2, and sums of squares residuals, while still sampling a sizable proportion of total site grid cells, which we define as > 25%. We applied linear regression without intercept values, comparing survey pair LAD profiles according to Model 3, repeating with different threshold values, and recorded statistics (Fig. 2). The same threshold was applied such that acceptable neighborhood cells met the pulse return density threshold requirement in both surveys. Since repeat LAD profiles were independent lidar-derived estimates, we applied reduced major axis regression (RMA) using the R package, "smatr" (Warton et al., 2012). The regression analysis was applied to every neighborhood grid cell individually and sensor-induced biases were interpreted as the deviations of the regression slope from one.

Prior work (Stark et al., 2012) determined a value of the MacArthur-Horn model LAD adjustment factor, *k*, for the Leica ALS50-II surveys (2008 DUC and TNF sites) that agreed with empirical leaf area measurements (see Section 3.2); thus, we set the bias correction factor of the Leica AL50-II to one. The bias correction factors applied to the other three sensors were then the mean values over neighborhood grid cells of RMA regression slopes against the LAD estimates of the Leica ALS50-II. As Optech ALTM Orion and Trimble Harrier 68i had no direct comparison with Leica ALS50-II, we carried through their comparisons with Optech ALTM 3100, and the comparison between Optech ALTM 3100 and Leica AL50-II, to indirectly calculate bias correction factors, to ultimately adjust all sensors to best estimate LAI.

3.5. Validation of sensor-induced bias correction

We validated sensor-induced bias correction by evaluating the consistency of bias correction factors. First, after calculating sensor-induced bias corrections (according to Model 3) for the 16 survey pairs, we tested for sensor pair effects with ANOVA and an associated Tukey's test to compare group differences. Sensor pairs were: ALTM Orion vs ALTM 3100 (5 survey pairs), ALTM 3100 vs Harrier 68i (3 pairs), ALTM Orion vs Harrier 68i (5 pairs), ALS50-II vs ALTM 3100 (3 pairs). Significant ANOVA results would suggest sensor-induced biases are consistent, while nonsignificant results would suggest that sensitivities are more likely attributable to survey or site specific variables, or random effects.

We also compared mean LAD profiles and LAI values of survey pairs before and after bias correction. In case mean neighborhood LAI values were more sensitive to potential site forest change, we also considered site maximum LAI values. Bias correction should move LAI mean and maximum values closer to one-to-one relationships.

3.6. Evaluation of biophysical change detection with corrected LAD profiles

After sensor-induced bias correction, we evaluated the potential for LAD profiles to reveal biophysical changes. We hypothesized that canopy gap formation would impact canopy surface height and LAD profiles, which we tested by comparing changes in canopy height with changes in leaf area density within height strata. In the 'Results' section, we summarized our findings from this approach, but it is detailed in Supplementary material in the 'Surface height and leaf area change' section. We also assessed whether LAD profile variation was consistent from one survey to the next at the 1/4 ha neighborhood grid scale. In the absence of canopy change, profile differences would represent measurement error; however, forest structural change also impacted differences since the interval between survey pairs was significant, ranging from 1 to 9 years. We hypothesized that if forest structural change is small annually, LAD profile variation should be highly consistent and increase with increasing between-survey intervals, or disturbance factors.

To test this hypothesis, we quantified LAD profile variation, and compared this over all survey pairs, with two complementary approaches. First, we regressed deviations from vertical profiles of survey pairs within each neighborhood cell, evaluating local regression performance *en masse*. Second, we constructed an overall regression for each survey pair comparing all deviations (e.g., all neighborhoods and all vertical positions) for a summary evaluation. Profile variation was calculated as deviations from consistent vertical trends (note that we calculated vertical trends specific to maximum canopy height to avoid potential artifacts). We fit RMA regressions to calculate statistics and regression slopes within each grid cell—high R^2 values and slopes close to 1 (and intercepts near zero) would indicate high detectability of neighborhood scale structural variation.

3.7. Survey parameters and sensor-induced biases

We asked if survey and sensor parameters (which varied consistently over devices in this dataset) were related to estimated biases. We related bias correction factors individually to lidar pulse beam divergence, footprint, altitude, scan angle and first return rates with Pearson correlation coefficients. We also applied this approach to assess potential correlations among sensor parameters. With a sample size of just four device pairs, however, inference was limited.

4. Results

4.1. Sensor-induced bias of LAD estimation

We found significant evidence of sensor-induced bias that was independent of pulse return density variation. Regressing LAD profiles between survey pairs in 1/4 ha neighborhood grid cells resulted in mean slope values that significantly differed from 1 in 15 out of 16 survey pairs (Table S2)—indicating sensor-induced biases, according to Model 3. More conservatively, testing *sensor pairs* using their *survey pairs* as replicates (i.e., any survey pair conducted with the same two sensors; N = 3 to 5; Table S2), two out of four cases appeared to significantly differ from 1, indicating sensor-induced bias, or, equivalently, different sensor 'sensitivities' to leaf area density (pair group *t*-test results in Table S2; ANOVA result: Df = 3; Sum Sq = 0.046; Mean Sq = 0.015; F value = 5.701; Pr = 0.012). Specifically, the Leica ALS-50 vs Optech ALTM 3100 pair differed from the ALTM Orion vs Harrier 68i pair (Pr < 0.05), and the ALS50-II vs ALTM 3100 pair trended towards difference with the ALTM 3100 vs Harrier 68i pair (Pr < 0.1).

After comparing sensors directly—and indirectly for ALTM Orion and Harrier 68i—to our standard, the ALS50-II (correction factor of 1), bias correction factors of the ALTM Orion, Harrier 68i, and ALTM 3100 were 1.077, 1.106 and 1.182, respectively (Fig. 3). Prior to correction, the ALTM 3100 estimated the smallest LAD values: on average, LAD estimates of the ALTM 3100 were 6.95%, 9.84% and 18.2% less than those of the Harrier 68i, ALTM Orion and ALS50-II, respectively (Figs. 3 and 4). Since ALTM Orion and Harrier 68i sensors had no direct comparison with the ALS50-II, bias correction factors were estimated indirectly via mutual comparison with the ALTM 3100. However, the ALTM Orion and Harrier 68i were compared directly to each other, and this allowed for a simple validation calculation: the Harrier 68i to ALTM Orion direct comparison estimated a bias of 2.52% (1.0252 bias factor). Constructing the same comparison indirectly, the bias is 2.70% (in terms of bias factors: 1.0984/1.0695 = 1.0270). Thus, direct and indirect paths are in close agreement (0.18% difference), suggesting internal consistency for the indirect calibration of these sensors.

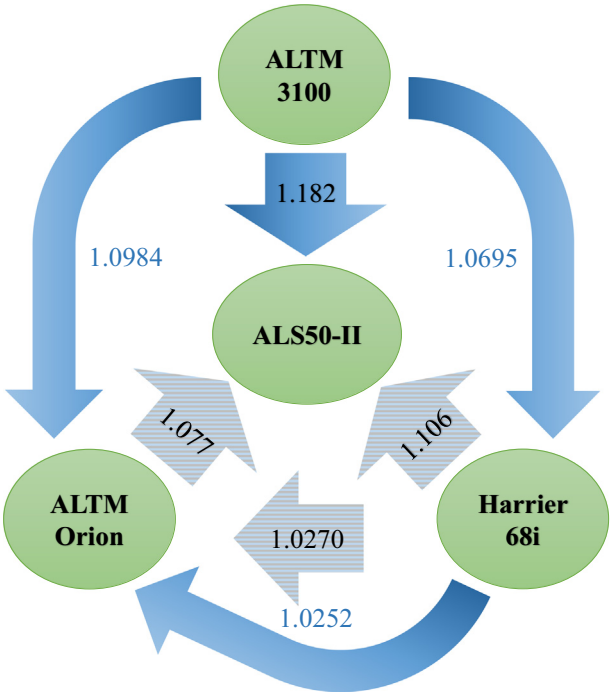

Fig. 3. Pairwise correction factors among all sensors. ALS50-II (center) is the reference (the correction factor of ALS50-II is 1), thus, the three arrows in the center pointing to ALS50-II are the correction factors used to make LAD comparable in this study. Blue arrows indicate direct estimates from sensor pairs available in our dataset; gray arrows show indirect estimates via multiple sensor comparisons, see details in Section 4.1. Comparing ALTM Orion and Harrier 68i, the direct and indirect estimated correction factors are 1.0252 and 1.0270, respectively, a difference of 0.18%. (For interpretation of the references to color in this figure legend, the reader is referred to the web version of this article.)

Regressions of second on first LAD estimates from survey pairs after correction were highly significant and predicted high proportions of variation (R^2: 0.73 to 0.96). Among the four pairwise combinations, the regression between ALTM 3100 and ALS50-II had the lowest R^2 (mean of 0.778) and largest residuals (mean of 0.017 $m^2 m^{-3}$; Table S2), but also the longest average survey interval (> 5 years). The other three combinations had similar and higher R^2 values, ranging from 0.885 to 0.920.

4.2. Pulse return density related bias

We found little evidence of pulse return density related biases. Fig. 4 reports the results of varying the minimum acceptable pulse return density sampling (i.e., pulse return density threshold) from 5 pts m^{-2} to 45 pts m^{-2} by 1 pts m^{-2} increments and recalculating the slope, R^2 values, residuals, and sample percentages (of acceptable grid cells) for each sensor pair. Pulse return density had little impact on these factors, particularly above 20 pts m^{-2} and when > 25% of grid cells were considered in analysis. For example, with increasing pulse return density, R^2 increased and residual values decreased initially, and then became stable at 20 pts m^{-2}, prior to major reductions in available grid cell percentages as the threshold reached high values. Thus, we selected 20 pts m^{-2} as our analysis threshold. Pulse return density thresholds that exceeded median grid cell values led to strong decreases in available grid cell percentages, causing drops below 25% between 25 and 40 pts m^{-2} for 3 out of the 4 sensor pairs. Regression slopes became unstable when the sampling percentage dropped below 20%. Reported in Supplementary material ('Direct pulse return density-related bias assessment'), we found that just 3.7% of differences (residuals) in survey pair profiles at the 1/4 ha grid cell level were explained by variation in pulse return density. Consistent with Model 3, pulse return density had effects on the uncertainties of regression analysis but not on LAD relationship slopes (sensor-induced biases).

4.3. LAD profiles and total LAI before and after correction

Fig. 5 presents mean vertical LAD profiles and standard errors for the TNF01 survey pair, before and after correction. Before correction, repeated LAD profile pairs had pronounced differences. After correction, differences were substantially reduced (compare Fig. 5 panels *a* and *b*). Fig. 6 shows corrected LAD profile comparisons for all 16 survey pairs, and pre-correction profiles are shown in Fig. S1. The majority of corrected LAD profile pair means and confidence regions overlapped each other without clear separation. LAD profile pairs with a short, single-year, interval between surveys had closer agreement than pairs with longer, multiple-year, survey intervals (see also interval effects in Section 4.4).

The comparison of survey pair LAI values was dramatically improved by sensor bias correction. Applying reduced major axis regression to LAI values of pairs before correction resulted in a low and nonsignificant R^2 of −0.181, with a root-mean-square error (RMSE) of 0.541 $m^2 m^{-2}$ (Fig. 7). After correction, the LAI comparison was highly significant, the R^2 increased to 0.824, and the RMSE decreased to 0.238 $m^2 m^{-2}$. The regression slope after correction was 0.995, close to a one-to-one relationship.

4.4. Detecting canopy change with LAD profiles

Reported in Fig. S2, we found varied relationships between LAD profile and canopy surface height changes at different vertical positions

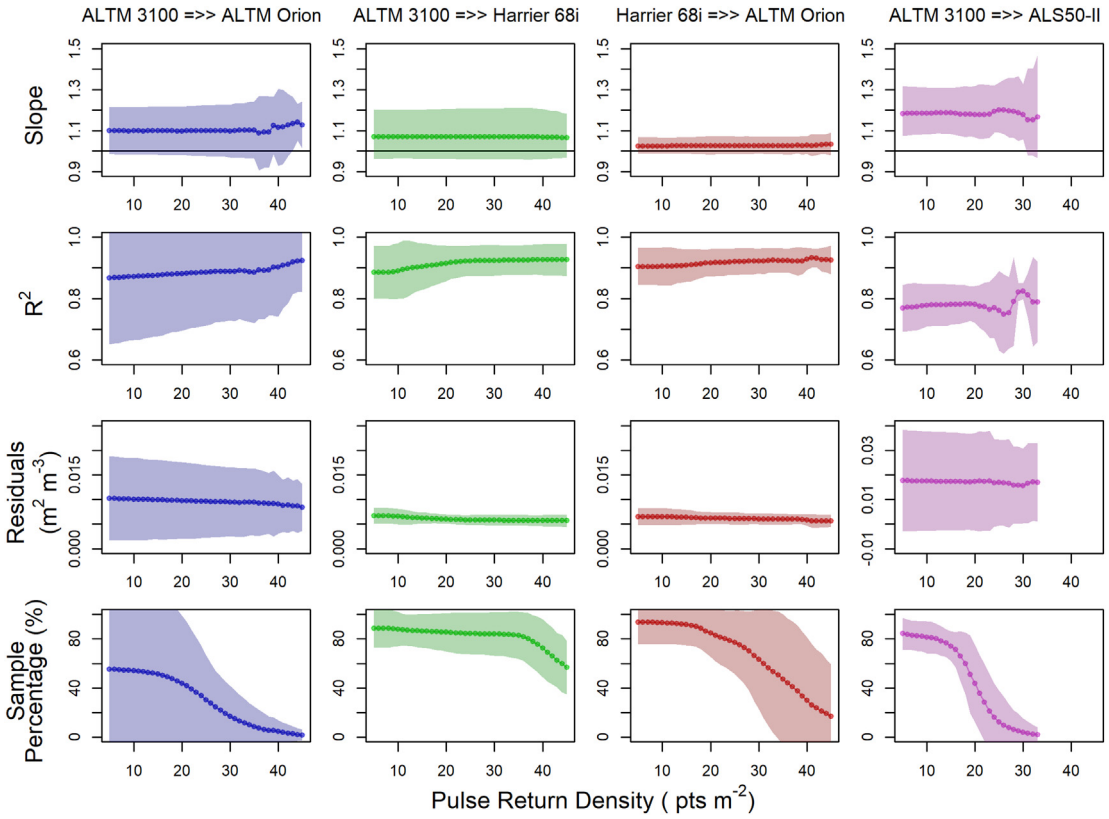

Fig. 4. The effects of pulse return density requirements on the calculation of sensor-induced biases. The colors show different sensor combinations: blue shows regression results matching ALTM 3100 to ALTM Orion; green ALTM 3100 to Harrier 68i; red Harrier 68i to ALTM Orion; purple ALTM 3100 to ALS50-II. Each statistic is presented with the mean value of each sensor combination group (dotted line) and the 95% confidence interval (colored region). (For interpretation of the references to color in this figure legend, the reader is referred to the web version of this article.)

in the canopy. Positive correlations were high in the upper portions of the canopy in a disturbed site (R^2 up to 0.805) but generally decreased to non-significant values near zero with increasing depth in the vegetation profile, and with decreasing disturbance impact over sites. See 'Surface height and leaf area change' in Supplementary material.

To assess the detectability of forest structure variation and change at 1/4 ha neighborhood scales, we compared survey pair LAD profile deviations from vertical trends. We regressed deviations from vertical profiles within each neighborhood grid cell, and, for a summary evaluation, all deviations (all neighborhoods and all vertical positions).

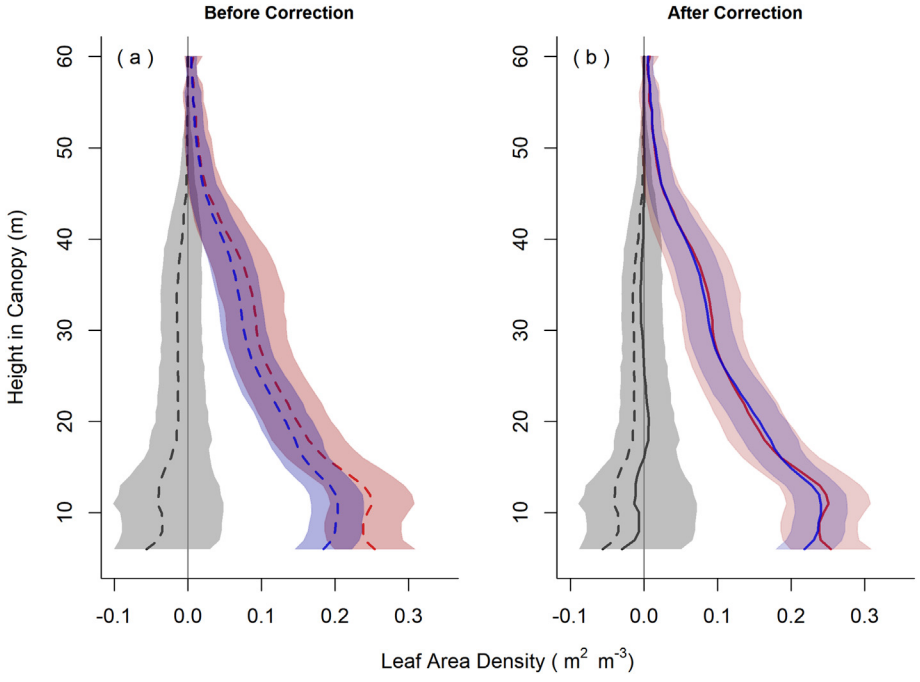

Fig. 5. Estimated leaf area density profiles of the TNF01 site (survey year 2008 vs 2012) before and after correction. Data has been filtered to areas with > 20 pulse returns m^{-2} and with canopy height changes not exceeding ± 2 m. Red colored confidence regions show the first survey and blue show the second. Gray regions are profile differences (dashed black line, before correction; solid black line, after correction). Figs. 6 and S1 show these same before and after correction profiles comparisons for all survey pairs. The reference profile is the 2008 TNF01 site survey. (For interpretation of the references to color in this figure legend, the reader is referred to the web version of this article.)

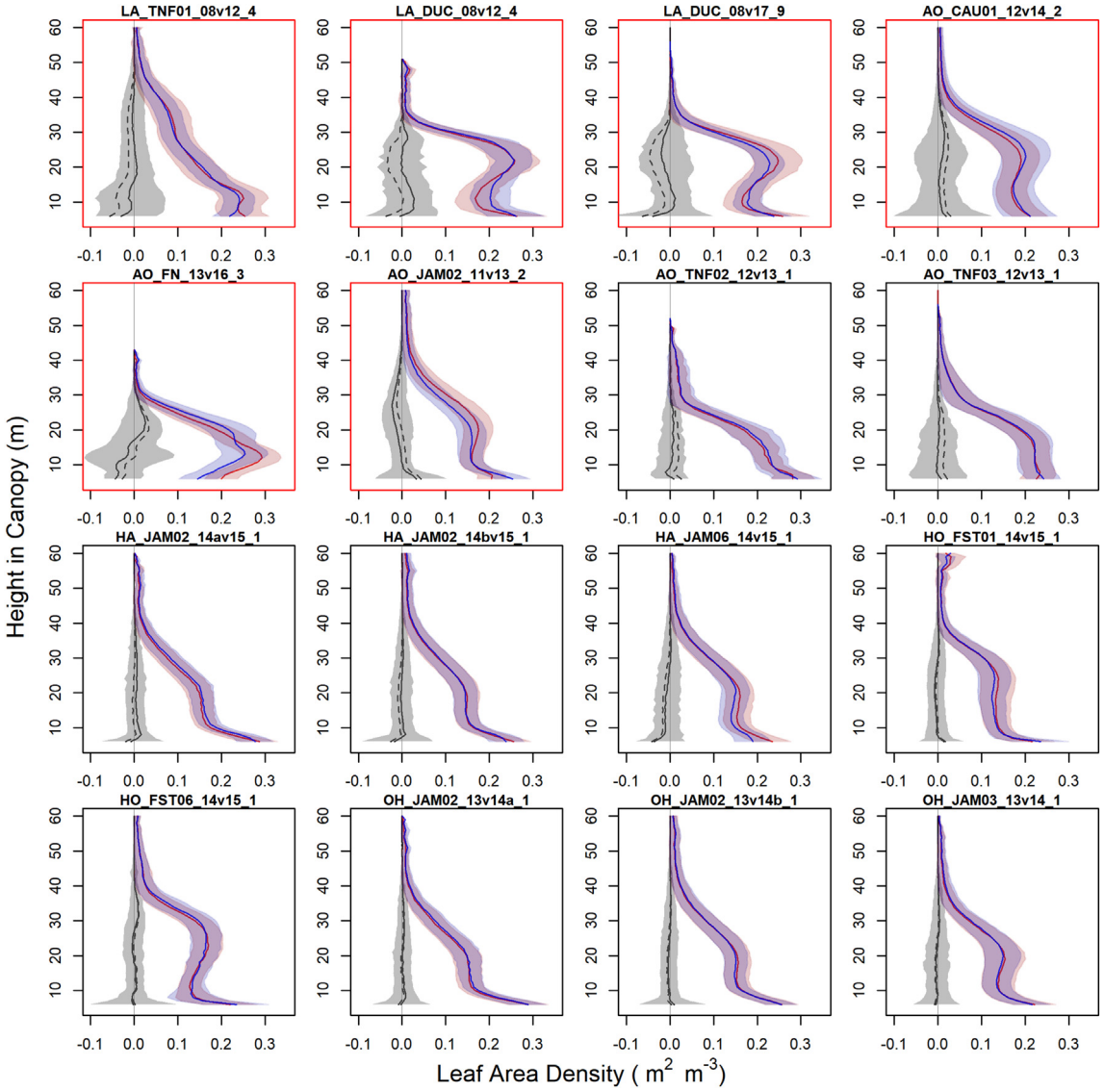

Fig. 6. Estimated leaf area density profiles of all sites after correction. Data are filter as in Fig. 5. Red confidence regions are first surveys and blue second surveys. Gray regions are profile differences (dashed black lines, before correction; solid black lines, after correction). Fig. S1 presents the same comparisons before correction. The reference profile is the 2008 survey in site TNF01. The subtitle of each subplot has four components separated by an underscore: the first indicates the laser sensor combination, where "L" is ALS50-II, "A" is ALTM 3100, "O" is ALTM Orion, and "H" is Harrier 68i; the second component is the site name (the number is the subsite index); the third component comprises the years of each survey in the pair separated by "v" ("a" and "b" indicate different survey regions within the same site in the same year); the fourth component is the resurvey interval in years (red bordered plots: multiple-year interval; black bordered plots: single-year interval). (For interpretation of the references to color in this figure legend, the reader is referred to the web version of this article.)

Regressions of all deviations were significant for all 16 survey pairs, with R^2 values ranging from 0.16 to 0.74, with a mean of 0.53. R^2 values were correlated with survey interval, decreasing as interval increased (Fig. 8; standard error = 0.140, R^2 = 0.516; 14 DF; p-value < 0.01). Standard deviations were also highly correlated with survey interval (Fig. 8; standard error = 0.00526; R^2 = 0.842; 14 DF; p-value < 0.001). LAD deviation correlations within 1/4 ha neighborhood cells were overwhelmingly significant: the percentages of grid cells with significant correlations at p-value ≤ 0.001 ranged from 53.8 to 99.6%, with a mean of 87.5% of grid cells. Percentages of significant grid cells were correlated with survey interval too, decreasing with increasing interval (standard error = 10.9; R^2 = 0.445; 14 DF; p-value < 0.01). The RMA regression slopes of relationships within grid cells, however, did not significantly vary with survey interval length, or mean R^2 values. RMA slopes ranged from 0.766 to 1.226 with a mean of 1.002 and a standard deviation of 0.113 (Fig. 9 lower right panel presents slopes for TNF01 neighborhoods spatially).

We present an example of the analysis of 1/4 neighborhood scale variable change at TNF for the 2008–2012 survey interval, based on the leaf area estimation and bias correction approach developed in this study (Fig. 9).

4.5. Potential impacts of survey parameters on sensor-induced biases

Among key sensor parameters, only footprint displayed a potential relationship with bias correction factors—trending positive in this case (R^2 = 0.91; 2 DF; p-value = 0.089). Thus, lidar sensors with larger footprints produced smaller LAD estimates, all else being equal. Fig. S3 reports all correlation coefficients between sensor-survey parameters and bias corrections. Scan angle went down as altitude increased (R^2 = 0.98; 2 DF; p-value = 0.018) and trended towards an increase with beam divergence (R^2 = 0.92; 2 DF; p-value = 0.076).

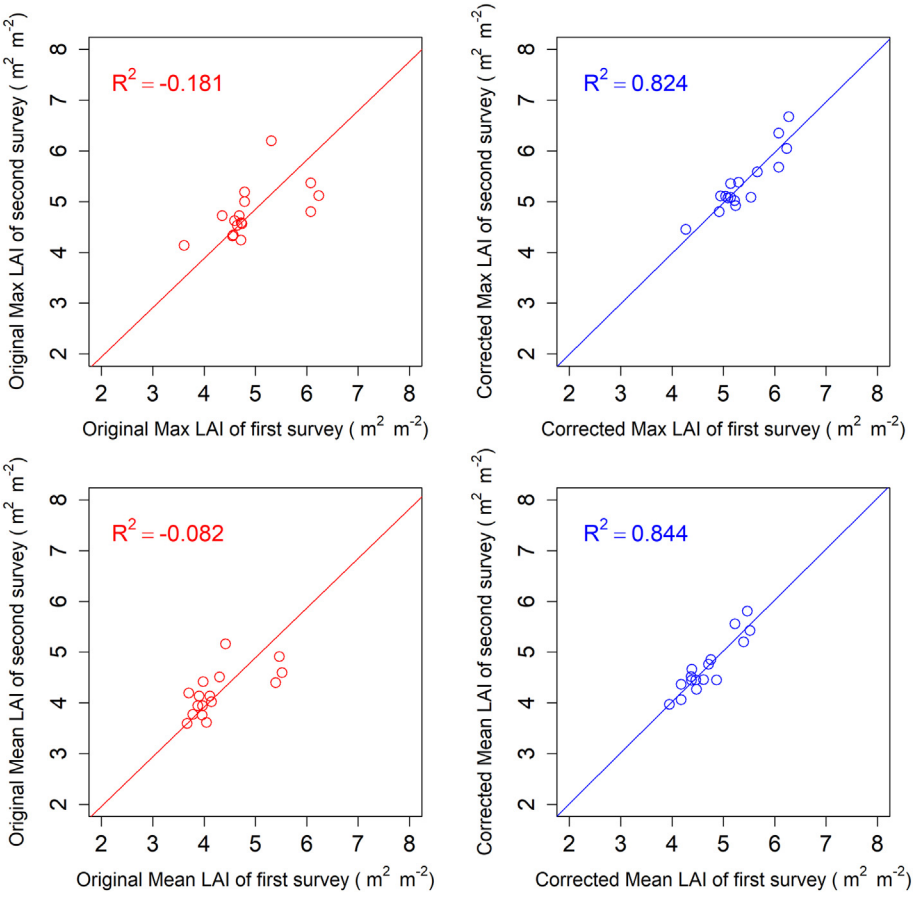

Fig. 7. Comparison of LAI estimations of all repeat survey pairs before (red) and after (blue) sensor-induced bias correction. Top panels show maximum LAI values, which are the 97% quantiles of all LAI 1/4 ha cell values within each survey (data filtered as in Figs. 5 and 6); the bottom panels show the same comparisons for mean LAI values. (For interpretation of the references to color in this figure legend, the reader is referred to the web version of this article.)

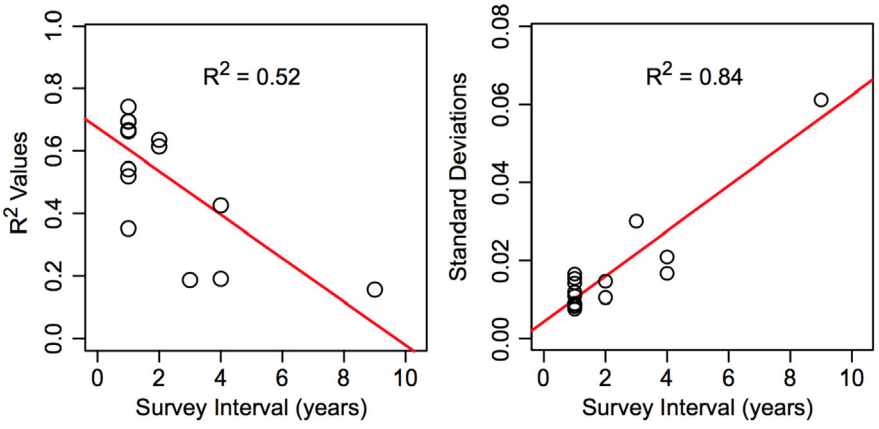

Fig. 8. Results of comparing height controlled grid cell LAD profile deviations between lidar survey pairs, showing R^2 values (left y axis) and standard deviations (right y axis), plotted against survey intervals (x axis). Shorter survey intervals have higher R^2 values and lower standard deviations, consistent with lower structural change.

5. Discussion

Our study provides strong evidence that a forest lidar database comprising multi-sensor and multitemporal surveys can monitor forest canopy structure through time and over geographical gradients with the accuracy needed to assess ecological changes. Systematic biases in leaf area index (LAI) and leaf area density (LAD) estimation were present and associated with lidar sensors. These biases could be assessed and corrected with a regression based approach, particularly when lidar sampling offered > 20 pulse returns m^{-2}. Our study also found strong support for the robust estimation of leaf area structure at forest neighborhood scales (1/4 ha grid cells); profile variation at this scale was consistent through time, with profile similarity decaying as interval length increased from one to nine years, consistent with expected impacts of forest dynamics and turnover. Lidar databases, while being well served by maximal standardization between surveys, can nonetheless succeed in the critical mission of monitoring changes in canopy structure in climatically important forests such as the Amazon under a range of sampling scenarios.

Our approach to quantifying leaf area variation, as well as assessing and reducing error in it, is unique and offers a foundation for future efforts. Validation and bias correction of lidar-based leaf area estimation with multiple sensors and varied collection parameters, over multiple sites, had not previously been undertaken. Instead, validation of multitemporal lidar surveys has primarily focused on upper canopy surfaces, specifically canopy height models (CHMs) (Zhao et al., 2018) used to monitor carbon dynamics (Cao et al., 2016; Shao et al., 2018a; Silva et al., 2017). And approaches to correct systematic bias between sensors have focused on a single forest site rather than an array of sites (Magnussen et al., 2010; Réjou-Méchain et al., 2015; Roussel et al.,

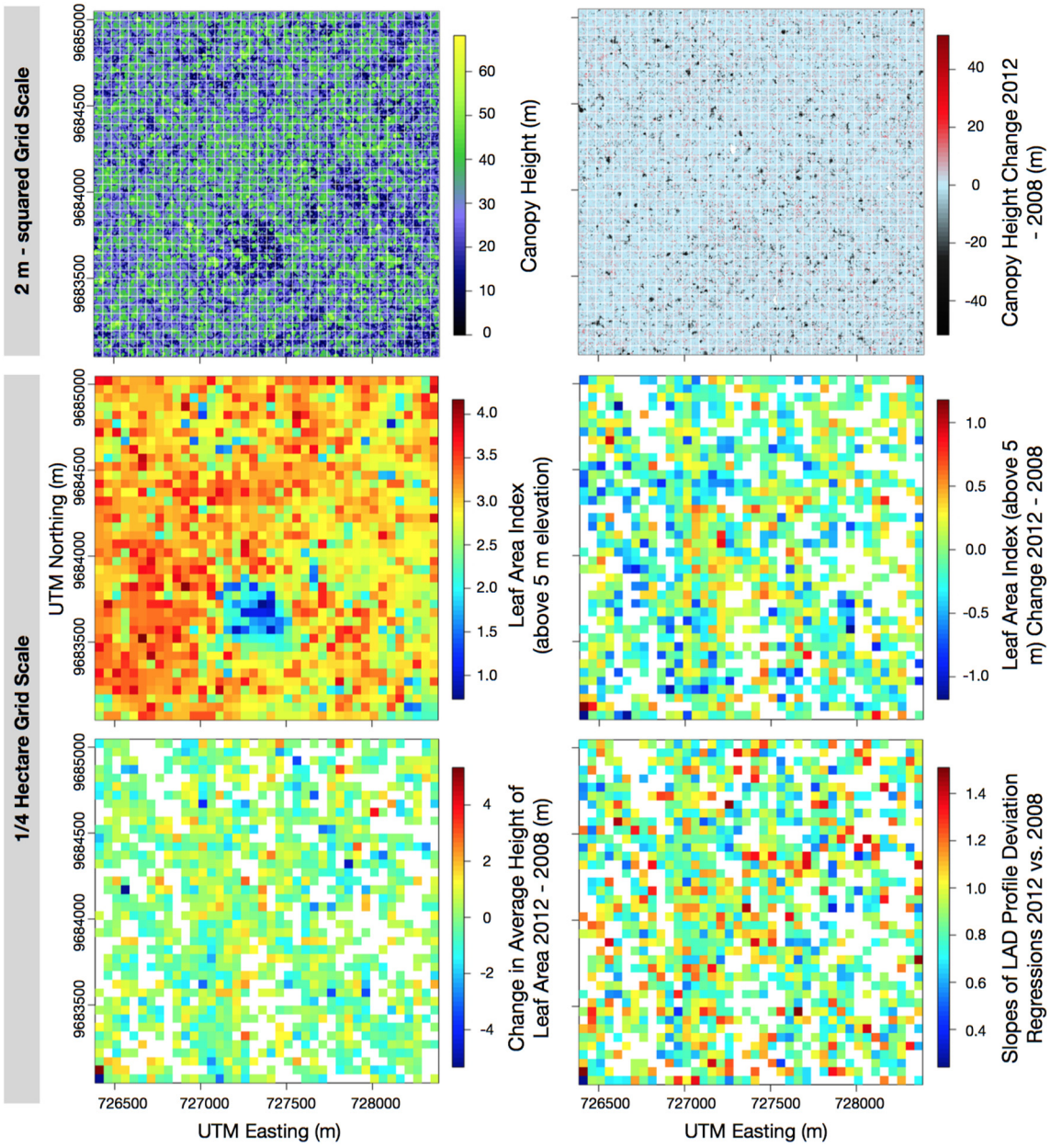

Fig. 9. Example of forest neighborhood analysis variables for TNF01 ("k67" flux tower site) comparing 2008 and 2012 lidar. The top two panels show 2 m^2 grid scale variables of forest canopy surface heights and surface height changes. White grid lines show divisions into 1/4 plot grid cells, the grid scale of the lower four panels. LAI from 2008 is presented with areas that fell below the pulse return density threshold filled with inverse distance weighted estimates; in LAI change and other panels, these areas appear as white spaces. The average height of leaf area is derived from LAD profiles (equivalent to LAD weighted height), and offers information about the vertical structure of vegetation change. The lowest right panel presents regression slopes resulting from cell-by-cell (1/4 ha neighborhood) comparison of LAD profile deviations from vertical trends, addressing the consistency of vertical structural variation over surveys. Here slopes were significantly positively related to LAI change, and closest to parity when LAI change was zero (standard error = 0.2981, R^2 = 0.148; 1075 DF; p-value < 0.001; outliers above 1.5 and below zero excluded).

2017).

5.1. Assessing leaf area structure through time and over space with multi-sensor airborne lidar

Comparing systematic variation of LAD estimates among four different airborne lidar systems, 16 repeated survey pairs, and over pulse return density gradients, our results demonstrated sensor-induced biases of lidar-derived LAD estimation. Sensor-induced biases impacted LAD values by up to 18.2%, and therefore would have a considerable effect on biophysical change analysis, and other ecological applications using multi-temporal lidar surveys. Fortunately, we found that sensor-induced biases could be estimated with linear regression analysis, and neutralized with bias correction factors (multipliers).

While it has long been appreciated that low sampling intensity—in this case, lidar pulse return density—can lead to leaf area estimation error in the active probe approach (MacArthur and Horn, 1969), we found little evidence of this over the spatial scales and sampling intensities of our analysis. We found that as long as pulse return density was above a sufficiently high threshold—20returns m^{-2}—LAD estimation bias was insensitive to this factor. Regression parameters showed low sensitivity to pulse return density (Fig. 4). If bias factors (Model 3 slopes), R^2 values, or residuals had been highly and consistently variable over pulse return density this would have been evidence for pulse

return density related bias. Instead, the regression parameters were effectively constant above the 20 pulses m^{-2} threshold and below the severe reductions in survey area that come with more-restrictive higher pulse return density thresholds. Direct regression of survey deviations of all neighborhood cells and all vertical positions on pulse densities (from both lidar surveys) offered mixed results (detailed in Supplementary material); here we found significant relationships, but these explained very small percentages of variation, < 4% on average with a maximum of 11%. Thus, our results are consistent with lidar sampling intensity playing a role in leaf area estimation error (MacArthur and Horn, 1969). But sampling intensity was not an appreciable source of bias over the sites or pulse densities considered. Prior studies, however, have described significant impacts of pulse return density on the quality of lidar metrics, particularly maximum canopy heights (Roussel et al., 2017; Zhao et al., 2018).

A unique aspect of our analysis was that it focused on the pulse return density variation within each dataset, whereas most previous studies focused on the pulse return density variation between datasets. This allowed us to analyze a large range of pulse densities (i.e., the density variation among grid cells ranged from 3 to over 100 pts m^{-2}). However, the pulse return density in our dataset, over 22 pts m^{-2} on average, is higher than the densities in most of the regional or national scale lidar surveys (typically ranging from 0.5 to 10 pts m^{-2}) (Wulder et al., 2012; Næsset et al., 2013; Shao et al., 2018b). To more comprehensively assess pulse return density related bias, a broader range of values will be needed in the future (e.g., expanding sampling to cover the 0.5–10 pts m^{-2} range).

Lidar survey parameters may have specific influences on LAD estimation. Among parameters, the laser footprint trended towards a relationship with correction factors, such that larger footprints appeared to produce smaller LAD estimates before correction (Fig. S3). While beam divergence was not significantly related to correction factors, we note that it is a key specification that influences other acquisition parameters. Larger beam divergence means lower beam energy, which may require lower flight altitude and wider scan angle to maintain footprint size and penetration rate, and the Sustainable Landscapes project acquisition parameters appear to vary in accordance with this constraint.

Future work could investigate the roles of survey parameters in leaf area estimation more rigorously, by varying the parameters of acquisitions in controlled contemporaneous resurveys. In this context, mechanistic explanations for the interaction between survey parameters and leaf area estimation may be explored; leaf area estimation is based on a light transfer analog, the MacArthur-Horn algorithm, that requires a sensitivity constant to scale pulse reflection probability to leaf area density. The influence of survey parameters on this constant may be understood ultimately as the interplay of optical properties of leaves and canopy structure and emission and detection components of the lidar, which could be investigated with dedicated survey designs.

Ecological variation over the Sustainable Landscapes study sites was apparent. After applying our calibration and validation approach we found that some sites had tall canopies but bottom-heavy leaf area profiles (e.g. TNF01), while others were shorter but had more LAD in the upper regions of the canopy (e.g. DUC; Stark et al., 2012), while yet others were intermediate between these extremes (e.g., JAM02).

5.2. Monitoring changing forest neighborhoods

Enhancing the capacity of lidar datasets to assess site-scale characteristics like the mean vertical LAD profile with validation and calibration will help reveal broad scale patterns of forest structure and change (Longo et al., 2016; Stark et al., 2012). The fine-scale heterogeneity of forest canopy structure contains unique and valuable ecological information on gap dynamics, forest demographic structure, microenvironmental variation, and other factors (Stark et al., 2012, 2015; Keller et al., 2004; Antonaraki et al., 2011; Hunter et al., 2015). Thus, we asked whether multitemporal multi-sensor lidar monitoring could identify 1/4 ha 'forest neighborhood' scale heterogeneity and change. When we compared the deviations of neighborhood LAD profiles from site means (controlled for local forest height) from successive lidar surveys we found that structural variation was highly consistent, i.e., variation was on average 60% predictable after one year. This was true whether we were considering all neighborhoods and strata at once, or analyzing neighborhood profiles one by one. Neighborhood profiles tended to be correlated, and had an average RMA regression slope of 1, indicating estimation parity, regardless of the length of interval between surveys. This demonstrated that site level bias correction results were also applicable at the neighborhood scale, allowing analysis and spatial interpretation of changes in canopy structure variables, which we show for TNF01 in Fig. 9.

Turnover in forest structure is an ongoing process that should act to reduce the similarity of any particular neighborhood with past states through time. Consistent with this, we observed a decline from > 60 to < 20% of variation in LAD profile deviations explained by prior surveys as the time interval between surveys increased from one year to nine years. Indeed, both anthropogenic and natural disturbances were at play through time at these sites, likely considerably impacting canopy structure (Fig. 8; Longo et al., 2016). A limitation of our study is that we cannot yet precisely offer uncertainty estimates for apparent changes between subsequent surveys in specific neighborhoods. Fitting either a linear, or nonlinear asymptotic function, to the time decay of predictability (R^2 values), however, offers a rough estimate, suggesting that resurvey error rates may be as high as 20 or 30% (based on the intercept at 'zero years,' Fig. 8; nonlinear fit not shown). In this case, there would be around a 10% change attributable to growth and dynamics after a year. Future longer-term resampling will offer better opportunities to partition error and turnover rates.

We hypothesized that canopy height changes, accurately detectable on the well-surveyed canopy surface of the forest, could help pinpoint LAD profile changes. The relationships between surface and LAD change in vertical strata were generally weak, however, and decreased with depth and forest stability (Fig. S2). Canopy surface change may still be useful for identifying forest dynamics, but our results suggest that significant variation in LAD change may be unrelated to canopy surface dynamics. Sub-canopy surface dynamics could explain this—subdominant trees and branches can grow, die, and fall all under taller canopy trees without impacting canopy surfaces.

6. Conclusions and implications for future research

Our study presents and evaluates a method to estimate total leaf area (LAI) and the vertical profile of leaf area density (LAD profiles) for sites, and 1/4 ha neighborhood grids within sites, from heterogenous multitemporal multi-sensor lidar databases. Our study confirmed systematic variation in leaf area estimation by laser systems—'sensor-induced biases'—and provided an effective and convenient comparative approach for correction. This approach relied on filtering to the highest quality survey data, with the lowest chance of canopy change, before regressing leaf area density estimates from subsequent surveys made with different sensors to quantify sensitivity as the slope of the relationship. Lidar pulse return density should exceed 20 points m^{-2} to enable accurate calibration and leaf area estimation, but values above this threshold did not have an important bias impact per se. The interval length between surveys did not appear to systematically impact bias detection, but shorter intervals should produce higher accuracy calibrations. Calibration also enabled characterization of 1/4 ha forest neighborhood heterogeneity, which displayed spatial variation that was highly detectable by multi-sensor lidar resurveys, though with regression statistics that varied by survey interval, reflecting the decay of forest similarity through time. Identifying significant leaf area changes on a 1/4 ha cell by cell basis remains a challenge, but can be aided by partial associations with canopy surface height changes and enhanced

error estimation in future work.

Our calibration approach offers robust estimation of patterns of leaf area variation at multiple spatial scales and should be undertaken for any comparative analysis—consider that prior to correction, LAI estimates from resurvey pairs were not related, while after correction the R^2 value jumped to > 0.8. This study demonstrates the feasibility and consistency of lidar to quantify key characteristics of leaf area structural variation with variable collections. Thus, lidar offers high throughput 3-D assessment of forest canopies, providing information beyond simple canopy surface height metrics that can be used to understand changing carbon cycles, forests dynamics and other functions in Amazonian forests, and likely elsewhere.

The Sustainable Landscapes Brazil dataset is of a high quality appropriate for fine-scaled ecological research due to high pulse return densities and other favorable scan characteristics. Future analysis could encompass surveys with lower pulse densities and higher scan angles to explore leaf area estimation bias in lower cost surveys. Prior calibration approaches have not considered an array of sites, survey systems, and sensors; however, given the need for coordinated monitoring to assess climate change effects on forest processes over broad scales—an objective shared by Sustainable Landscapes and the National Ecological Observatory Network (NEON) in the United States—we expect future efforts to increasingly incorporate heterogeneous multi-sensor lidar datasets. Our study suggests that increased understanding of the factors that influence lidar based leaf area estimation and comparisons of lidar systems through site resurveys—including with no time interval to isolate measurement error—can support these efforts and critically improve hypothesis testing. Ground collected leaf area profiles (see Clark et al., 2008) from multiple locations and paired with airborne lidar surveys are required to validate this method with the highest rigor, and should not be overlooked as a funding priority, while ground based lidar systems may offer additional validation opportunities (Stark et al., 2012).

Acknowledgements

We thank the Sustainable Landscapes Brazil project for providing the lidar data. D. Almeida was supported by the São Paulo Research Foundation (#2017/03867-6 and #2016/05219-9), S. C. Stark by NSF (EF-1550686, EF-1340604, and EF-1702379). Veronika Leitold provided data visualization assistance.

Appendix A. Supplementary material

Supplementary material to this article can be found online at https://doi.org/10.1016/j.rse.2018.10.035.

References

Aber, J.D., 1979. A method for estimating foliage-height profiles in broad-leaved forests. J. Ecol. 67 (1), 35–40.
Allen, C.D., Breshears, D.D., McDowell, N.G., 2015. On underestimation of global vulnerability to tree mortality and forest die-off from hotter drought in the Anthropocene. Ecosphere 6 (8), 1–55.
Antonarakis, A.S., Saatchi, S.S., Chazdon, R.L., Moorcroft, P.R., 2011. Using Lidar and Radar measurements to constrain predictions of forest ecosystem structure and function. Ecol. Appl. 21 (4), 1120–1137.
Antonarakis, A.S., Munger, J.W., Moorcroft, P.R., 2014. Imaging spectroscopy- and lidar-derived estimates of canopy composition and structure to improve predictions of forest carbon fluxes and ecosystem dynamics. Geophys. Res. Lett. 41, 2535–2542.
Asner, G.P., Knapp, D.E., Kennedy-Bowdoin, T., Jones, M.O., Martin, R.E., Boardman, J.W., Field, C.B., 2007. Carnegie airborne observatory: in-flight fusion of hyperspectral imaging and waveform light detection and ranging for three-dimensional studies of ecosystems. J. Appl. Remote. Sens. 1 (1), 013536.
Bonan, G.B., 2008. Forests and climate change: forcings, feedbacks, and the climate benefits of forests. Science 320 (5882), 1444–1449 (Jun 13).
Bonan, G., 2015. Ecological Climatology: Concepts and Applications. Cambridge University Press.
Cao, L., Coops, N.C., Innes, J.L., Sheppard, S.R., Fu, L., Ruan, H., She, G., 2016. Estimation of forest biomass dynamics in subtropical forests using multi-temporal airborne LiDAR data. Remote Sens. Environ. 178, 158–171.
Chambers, J.Q., Asner, G.P., Morton, D.C., Anderson, L.O., Saatchi, S.S., Espírito-Santo, F.D.B., Palace, M., Souza, C., 2007. Regional ecosystem structure and function: ecological insights from remote sensing of tropical forests. Trends Ecol. Evol. 22, 414–423.
Clark, D.B., Olivas, P.C., Oberbauer, S.F., Clark, D.A., Ryan, M.G., 2008. First direct landscape-scale measurement of tropical rain forest Leaf Area Index, a key driver of global primary productivity. Ecol. Lett. 11, 163–172.
Davidson, E.A., de Araújo, A.C., Artaxo, P., Balch, J.K., Brown, I.F., Bustamante, M.M., Coe, M.T., DeFries, R.S., Keller, M., Longo, M., Munger, J.W., 2012. The Amazon basin in transition. Nature 481 (7381), 321.
Detto, M., Asner, G.P., Muller-Landau, H.C., Sonnentag, O., 2015. Spatial variability in tropical forest leaf area density from multireturn lidar and modeling. J. Geophys. Res. Biogeo. 120, 294–309.
Fisher, R., Williams, M., Costa, D., Lola, A., Malhi, Y., da Costa, R., Almeida, S., Meir, P., 2007. The response of an Eastern Amazonian rain forest to drought stress: results and modelling analyses from a throughfall exclusion experiment. Glob. Chang. Biol. 13, 2361–2378.
Foley, J.A., Asner, G.P., Costa, M.H., Coe, M.T., DeFries, R., Gibbs, H.K., Howard, E.A., Olson, S., Patz, J., Ramankutty, N., 2007. Amazonia revealed: forest degradation and loss of ecosystem goods and services in the Amazon Basin. Front. Ecol. Environ. 5, 25–32.
Garcia, E.S., Swann, A.L., Villegas, J.C., Breshears, D.D., Law, D.J., Saleska, S.R., Stark, S.C., 2016. Synergistic ecoclimate teleconnections from forest loss in different regions structure global ecological responses. PLoS One 11, e0165042.
Guo, T., Engel, B.A., Shao, G., Arnold, J.G., Srinivasan, R., Kiniry, J.R., 2015. Functional approach to simulating short-rotation woody crops in process-based models. Bioenergy Res. 8, 1598–1613.
Hansen, M.C., Potapov, P.V., Moore, R., Hancher, M., Turubanova, S.A.A., Tyukavina, A., Thau, D., Stehman, S.V., Goetz, S.J., Loveland, T.R., Kommareddy, A., 2013. High-resolution global maps of 21st-century forest cover change. Science 342 (6160), 850–853.
Harding, D.J., Blair, J., Garvin, J.B., Lawrence, W.T., 1994. Laser altimetry waveform measurement of vegetation canopy structure. In: Geoscience and Remote Sensing Symposium, 1994. IGARSS'94. Surface and Atmospheric Remote Sensing: Technologies, Data Analysis and Interpretation, International. IEEE, pp. 1251–1253.
Hilker, T., Lyapustin, A.I., Tucker, C.J., Hall, F.G., Myneni, R.B., Wang, Y., Bi, J., de Moura, Y.M., Sellers, P.J., 2014. Vegetation dynamics and rainfall sensitivity of the Amazon. Proc. Natl. Acad. Sci. 111 (45), 16041–16046.
Hosoi, F., Nakai, Y., Omasa, K., 2010. Estimation and error analysis of woody canopy leaf area density profiles using 3-D airborne and ground-based scanning lidar remote-sensing techniques. IEEE Trans. Geosci. Remote Sens. 48, 2215–2223.
Hunter, M.O., Keller, M., Morton, D., Cook, B., Lefsky, M., Ducey, M., Saleska, S., de Oliveira Jr., R.C., Schietti, J., 2015. Structural dynamics of tropical moist forest gaps. PLoS One 10 (7), e0132144.
Jakubowski, M.K., Guo, Q., Kelly, M., 2013. Tradeoffs between lidar pulse density and forest measurement accuracy. Remote Sens. Environ. 130, 245–253.
Keller, M., Alencar, A., Asner, G.P., Braswell, B., Bustamante, M., Davidson, E., Feldpausch, T., Fernandes, E., Goulden, M., Kabat, P., Kruijt, B., 2004. Ecological research in the large-scale biosphere–atmosphere experiment in Amazonia: early results. Ecol. Appl. 14 (sp4), 3–16.
Knapp, N., Fischer, R., Huth, A., 2018. Linking lidar and forest modeling to assess biomass estimation across scales and disturbance states. Remote Sens. Environ. 205, 199–209.
Lefsky, M.A., Cohen, W.B., Parker, G.G., Harding, D.J., 2002. Lidar remote sensing for ecosystem studies: Lidar, an emerging remote sensing technology that directly measures the three-dimensional distribution of plant canopies, can accurately estimate vegetation structural attributes and should be of particular interest to forest, landscape, and global ecologists. Bioscience 52 (1), 19–30.
Liu, J., Skidmore, A.K., Jones, S., Wang, T., Heurich, M., Zhu, X., Shi, Y., 2018. Large off-nadir scan angle of airborne LiDAR can severely affect the estimates of forest structure metrics. ISPRS J. Photogramm. Remote Sens. 136, 13–25.
Longo, M., Keller, M., dos-Santos, M.N., Leitold, V., Pinagé, E.R., Baccini, A., Saatchi, S., Nogueira, E.M., Batistella, M., Morton, D.C., 2016. Aboveground biomass variability across intact and degraded forests in the Brazilian Amazon. Glob. Biogeochem. Cycles 30, 1639–1660.
MacArthur, R.H., Horn, H.S., 1969. Foliage profile by vertical measurements. Ecology 50, 802–804.
Magnussen, S., Næsset, E., Gobakken, T., 2010. Reliability of LiDAR derived predictors of forest inventory attributes: a case study with Norway spruce. Remote Sens. Environ. 114 (4), 700–712.
Malhi, Y., Roberts, J.T., Betts, R.A., Killeen, T.J., Li, W., Nobre, C.A., 2008. Climate change, deforestation, and the fate of the Amazon. Science 319, 169–172.
McDowell, N.G., Coops, N.C., Beck, P.S., Chambers, J.Q., Gangodagamage, C., Hicke, J.A., Huang, C.Y., Kennedy, R., Krofcheck, D.J., Litvak, M., Meddens, A.J., 2015. Global satellite monitoring of climate-induced vegetation disturbances. Trends Plant Sci. 20 (2), 114–123.
Morsdorf, F., Frey, O., Meier, E., Itten, K.I., Allgöwer, B., 2008. Assessment of the influence of flying altitude and scan angle on biophysical vegetation products derived from airborne laser scanning. Int. J. Remote Sens. 29 (5), 1387–1406.
Næsset, E., Gobakken, T., Bollandsås, O.M., Gregoire, T.G., Nelson, R., Ståhl, G., 2013. Comparison of precision of biomass estimates in regional field sample surveys and airborne LiDAR-assisted surveys in Hedmark County, Norway. Remote Sens. Environ. 130, 108–120.
Olivas, P.C., Oberbauer, S.F., Clark, D.B., Clark, D.A., Ryan, M.G., O'Brien, J.J., Ordonez, H., 2013. Comparison of direct and indirect methods for assessing leaf area index across a tropical rain forest landscape. Agric. For. Meteorol. 177, 110–116.
Parker, G.G., Harding, D.J., Berger, M.L., 2004a. A portable LIDAR system for rapid

determination of forest canopy structure. J. Appl. Ecol. 41, 755–767.
Parker, G.G., Harmon, M.E., Lefsky, M.A., Chen, J., Pelt, R.V., Weis, S.B., Thomas, S.C., Winner, W.E., Shaw, D.C., Frankling, J.F., 2004b. Three-dimensional structure of an old-growth Pseudotsuga-Tsuga canopy and its implications for radiation balance, microclimate, and gas exchange. Ecosystems 7, 440–453.
Phillips, O.L., Aragão, L.E., Lewis, S.L., Fisher, J.B., Lloyd, J., López-González, G., Malhi, Y., Monteagudo, A., Peacock, J., Quesada, C.A., Van Der Heijden, G., 2009. Drought sensitivity of the Amazon rainforest. Science 323 (5919), 1344–1347.
R Development Core Team, v3.3.2, 2013. R: A Language and Environment for Statistical Computing.
Réjou-Méchain, M., Tymen, B., Blanc, L., Fauset, S., Feldpausch, T.R., Monteagudo, A., Phillips, O.L., Richard, H., Chave, J., 2015. Using repeated small-footprint LiDAR acquisitions to infer spatial and temporal variations of a high-biomass Neotropical forest. Remote Sens. Environ. 169, 93–101.
Roussel, J.R., Caspersen, J., Béland, M., Thomas, S., Achim, A., 2017. Removing bias from LiDAR-based estimates of canopy height: accounting for the effects of pulse density and footprint size. Remote Sens. Environ. 198, 1–16.
Saleska, S.R., Didan, K., Huete, A.R., Da Rocha, H.R., 2007. Amazon forests green-up during 2005 drought. Science 318 (5850), 612-612.
Shao, G., Shao, G., Gallion, J., Saunders, M.R., Frankenberger, J.R., Fei, S., 2018a. Improving Lidar-based aboveground biomass estimation of temperate hardwood forests with varying site productivity. Remote Sens. Environ. 204, 872–882.
Shao, G., Iannone, B.V., Fei, S., 2018b. Enhanced forest interior estimations utilizing lidar-assisted 3D forest cover map. Ecol. Indic. 93, 1236–1243.
Silva, C.A., Hudak, A.T., Vierling, L.A., Klauberg, C., Garcia, M., Ferraz, A., Keller, M., Eitel, J., Saatchi, S., 2017. Impacts of airborne lidar pulse density on estimating biomass stocks and changes in a selectively logged tropical forest. Remote Sens. 9 (10), 1068.
Stark, S.C., Leitold, V., Wu, J.L., Hunter, M.O., de Castilho, C.V., Costa, F.R., McMahon, S.M., Parker, G.G., Shimabukuro, M.T., Lefsky, M.A., 2012. Amazon forest carbon dynamics predicted by profiles of canopy leaf area and light environment. Ecol. Lett. 15, 1406–1414.
Stark, S.C., Enquist, B.J., Saleska, S.R., Leitold, V., Schietti, J., Longo, M., Alves, L.F., Camargo, P.B., Oliveira, R.C., 2015. Linking canopy leaf area and light environments with tree size distributions to explain Amazon forest demography. Ecol. Lett. 18, 636–645.
Stark, S.C., Breshears, D.D., Garcia, E.S., Law, D.J., Minor, D.M., Saleska, S.R., Swann, A.L., Villegas, J.C., Aragão, L.E., Bella, E.M., Borma, L.S., 2016. Toward accounting for ecoclimate teleconnections: intra-and inter-continental consequences of altered energy balance after vegetation change. Landsc. Ecol. 31 (1), 181–194.
Tang, H., Dubayah, R., Swatantran, A., Hofton, M., Sheldon, S., Clark, D.B., Blair, B., 2012. Retrieval of vertical LAI profiles over tropical rain forests using waveform lidar at La Selva, Costa Rica. Remote Sens. Environ. 124, 242–250.
Tang, H., Ganguly, S., Zhang, G., Hofton, M., Nelson, R., Dubayah, R., 2016. Characterizing leaf area index (LAI) and vertical foliage profile (VFP) over the United States. Biogeosciences 13, 239.
Véga, C., Renaud, J.-P., Durrieu, S., Bouvier, M., 2016. On the interest of penetration depth, canopy area and volume metrics to improve Lidar-based models of forest parameters. Remote Sens. Environ. 175, 32–42.
Vincent, G., Antin, C., Laurans, M., Heurtebize, J., Durrieu, S., Lavalley, C., Dauzat, J., 2017. Mapping plant area index of tropical evergreen forest by airborne laser scanning. A cross-validation study using LAI2200 optical sensor. Remote Sens. Environ. 198, 254–266.
Warton, D.I., Duursma, R.A., Falster, D.S., Taskinen, S., 2012. smatr 3–an R package for estimation and inference about allometric lines. Methods Ecol. Evol. 3 (2), 257–259.
Weiss, M., Baret, F., Smith, G., Jonckheere, I., Coppin, P., 2004. Review of methods for in situ leaf area index (LAI) determination: part II. Estimation of LAI, errors and sampling. Agric. For. Meteorol. 121, 37–53.
Wulder, M.A., White, J.C., Nelson, R.F., Næsset, E., Ørka, H.O., Coops, N.C., Hilker, T., Bater, C.W., Gobakken, T., 2012. Lidar sampling for large-area forest characterization: a review. Remote Sens. Environ. 121, 196–209.
Zhao, K., Suarez, J.C., Garcia, M., Hu, T., Wang, C., Londo, A., 2018. Utility of multitemporal lidar for forest and carbon monitoring: tree growth, biomass dynamics, and carbon flux. Remote Sens. Environ. 204, 883–897.
Zheng, G., Moskal, L.M., 2009. Retrieving leaf area index (LAI) using remote sensing: theories, methods and sensors. Sensors 9, 2719–2745.